Recent trends in wind-wave climate for the Indian Ocean

Nitika Gupta[1], Prasad K. Bhaskaran[1,*] and Mihir K. Dash[2]

[1]Department of Ocean Engineering and Naval Architecture, and
[2]Centre for Oceans, Rivers, Atmosphere and Land Sciences, Indian Institute of Technology, Kharagpur 721 302, India

Surface gravity waves play an important role in ocean engineering studies and their influence on the dynamics of the coastal zone is critical. Proper knowledge on wind-wave climatology is an area of immense interest to engineers and climate modellers. Climate change has influenced weather patterns over global oceans and at present is a matter of serious concern, as it can have long-term repercussions. There is a need to understand the recent trends in variability of wind-waves for planning operations. To improve climate projections the Intergovernmental Panel on Climate Change report highlights the need and importance for wind-wave climate study. With this motivation, we study the variability of recent trends in maximum wind speed (MWS) and maximum significant wave height (MSWH) exclusively based on altimeter data for the Indian Ocean basin. We use daily data of MWS and MSWH from eight satellite missions covering a period of 21 years (1992–2012). The findings indicate that regions in the Southern Ocean (between 45°S and 55°S) experienced the largest variability in wind-wave climate. Higher MSWH resulting from increased MWS has practical implications on swell generation field that eventually cross the hemisphere influencing wind-waves elsewhere. The study also reveals the impact of wind-wave activity for the Indian Ocean basin in the past decade.

Keywords: Climate, Indian Ocean, maximum wave height, maximum wind speed, satellite observations.

SATELLITES have played an important role during the past two decades as ocean observing systems. Data measured by satellites have improved our understanding of the evolution and variability of meteorological and surface oceanographic parameters such as wind speed, significant wave height, sea-surface temperature (SST), surface salinity, etc. Considerable progress has been made to understand the changes in weather patterns over land and oceans over time whereas the knowledge to understand the variability over short-time climate scales (in the order of few decades) is still in the formative stages. Prior to the advent of radar altimeters, few moored instruments recorded observations over the oceans off Europe, Japan and North America. The visual estimates from voluntary ships supplement these observations. Considering the vast expanse of the oceans, the location-specific observations along with the reports from ships were sparse to help understand the variability of meteorological and oceanographic parameters in basin scales. In addition, the information on the consistency and data quality from ship reports were questionable[1]. The advent of radar altimeter led to consistent measurement of maximum significant wave height and wind speed across the globe. At present, satellites provide an opportunity to understand the dynamic processes, basin scale features and long-term trends in the ocean environment. This has more advantage compared to *in situ* observing platforms, as they have ability to map large spatial areas. The wealth of the data obtained in recent times from multi-satellite borne platforms, facilitates quantifications of the spatio-temporal variations in atmosphere, land and ocean systems.

Initial work utilizing satellite data confines to mapping wave climate and studying on their seasonal variations. Longer data records provided an opportunity to understand the inter-annual variability[2,3]. In global perspective, the practical use of altimeter data to understand wind-wave climate started with the launch of GEOS-3 in 1975 (ref. 4) and SEASAT in 1978. Chelton *et al.*[5] released the first picture of wind-wave climate for global oceans. Later, Challenor *et al.*[6] and Carter *et al.*[7] used GEOSAT data to understand the seasonal and inter-annual variability of the wave climate. In a recent study[8], one can find a lucid illustration and review of a few important discoveries on the climate system that are undetected through climate models and conventional based observations. The authors highlight the role of satellites in understanding spatial patterns in sea-level rise and the cooling effect induced by increased aerosols in the upper atmosphere. One can find very few studies conducted for the trends in wind-wave climate projections. The few studies were on the Atlantic and Pacific Ocean basins[9] and not much is mentioned on the Indian Ocean. The only work available utilizing satellite measurements is by Hemer *et al.*[2], on the past wave climate based on inter-annual variability and trends associated with directional behaviour of ocean waves for the Southern Ocean (SO) sector.

Past studies such as Young *et al.*[3] examined the global trends in wind-wave climate. Wang *et al.*[10] used regression models based on redundancy analysis to understand

*For correspondence. (e-mail: prasadlsu@yahoo.com)

the relationship between sea level pressure (SLP) and significant wave height (SWH) for the North Atlantic Ocean. Projections of SWH for the northeast Atlantic in the 21st century using different forcing scenarios showed an increased tendency of SWH during both winter and fall seasons[10,11]. Similarly, for the Pacific basin, Shimura *et al.*[12] reported extreme values of future SWH and associated wind speed in tropical cyclone zones with both having a zonal dependence. Mori *et al.*[13] examined the projection of extreme wind-wave climate under global warming for the Japan Sea. For the Dutch coast in the North Sea region, Renske *et al.*[14] reported the effect of climate change on extreme waves, suggesting a possible increase in the annual wind-wave maxima and their effect on the coastal environment. The inferences from the above-mentioned studies are obtained from model simulations that are prone to errors from physical mechanisms such as downscaling methodology, wave-model physics, model forcing mechanisms, etc. This means, one can ensure measurement from satellites as the best choice to obtain a clear picture and realistic inference on basin-scale features for wind-wave variability. The objective of the present study is to analyse and quantify the trends in maximum SWH and maximum wind speed, and to identify the zones of maximum variability in the Indian Ocean basin, especially during fair weather conditions. The study focuses on understanding the inter-annual variations in wind-wave climate. Changing frequency and intensity of depressions and cyclones is an integral part of the climate system. However, the effect of climate change on the frequency and cyclone intensity is not within the scope of this study. Hence, extreme weather events like depressions and cyclones that have occurred in the past 21 years (1992–2012) do not form a part of this analysis. The present study utilizes data from eight satellite missions for this 21 years period.

Role of southern ocean on wind-wave climate

SO has a significant role in governing the wave climatology for global oceans. The extra-tropical belt in the Southern Hemisphere is an active region known for its potential for swell generation. Long waves (swells) generated from this region travel thousands of kilometers over global oceans reaching various destinations and crossing the hemisphere, thereby influencing the local wind-waves of that region[15]. Sterl and Caires[16] used empirical orthogonal function (EOF) analysis with ERA-40, re-analysed SWH data and reported that 15% of the global wave activity was due to swell propagation from the SO basin. Therefore, the SO plays an important role in governing the variability of the global mean wave height. To understand the principal drivers of variability, Hemer *et al.*[2] studied the inter-annual climate variability and the trends in the directional behaviour of wind-wave climate for SO basin, using data from satellite altimeters and global wave models. They used altimeter data from GEOSAT, ERS-1/2, TOPEX/Poseidon, JASON, ENVISAT and GFO missions. The source of data was from TuDelft RADS database[17]. The inter-annual trends and dominant modes of variability from altimeter using EOF analysis indicate a strong positive correlation between SWH in SO and Southern Annular Mode (SAM) during austral autumn and winter months[2]. From the perspective of climate, the wave climate variability in the Indian Ocean sector of SO correlated well with SAM, whereas a strong correlation was found between the altimeter derived SWH and Southern Ocean Index (SOI) for the Pacific basin. In another study, Young *et al.*[3] demonstrated the global trends in wind speed and wave height using altimeter measurements (wave height data from 1985 to 2008 and wind speed data from 1991 to 2008 were used). Their analysis covered three statistical parameters such as monthly mean and 90th and 99th percentile trend values for global oceans. The results signify an increasing trend for wind speed, and to a lesser extent for wave heights. An interesting observation was that the mean and the 90th percentile of the wind speed trends were similar, whereas an increased magnitude was noticed for the 99th percentile. This means that the intensity of extreme weather events increased at a faster rate compared to the mean conditions. The mean and 90th percentile analysis indicated that wind speed over vast stretches in global ocean has increased at a rate of 0.25% to 0.5% per year. A net increase of about 5–10% in the past 20 years has occurred with a stronger trend observed in the Southern Hemisphere compared to the Northern Hemisphere. They also indicate that monthly mean wave heights show no clear significant statistical trend. As pointed out earlier, it is worthwhile to note the statistical trend for the maximum SWH for the Indian Ocean and therefore the same was attempted in the present study.

Data and methodology

This study uses daily altimeter maximum significant wave height data from eight satellite missions for 21 years. The measured data from satellites use advanced microwave techniques that enable data coverage irrespective of cloud and sunlight conditions. The eight missions cover satellite data from ERS-1/2, TOPEX/Poseidon, GEOSAT Follow-ON (GFO), JASON-2, ENVISAT and CRYOSAT. The altimeter data used is a quality-checked product[18], and the corrected altimeter data available as daily data files were used for analysis. Table 1 lists the details of the eight satellite missions covering aspects on satellite passes and the data collection time. The ERS-1 data from European Space Agency (ESA) Radar altimeter Ocean product (OPR) for phase 'C' and 'G' has a 35-day repeat

Table 1. Geophysical data records used in the present study

Satellite	Product	Cycles	Time period	Remarks
ERS-1	OPR	Not defined	1 August 1991 to 30 March 1992	Phases A & B 3-days
		83 to 101	14 April 1992 to 20 December 1993	Phase C 35-days
		Not defined	24 December 1993 to 10 April 1994	Phase D 3-days
		Not defined	10 April 1994 to 21 March 1995	Phases E & F 168-days
		144 to 156	24 March 1995 to 2 June 1996	Phase G 35-days
ERS-2	OPR	1 to 169	15 May 1995 to 4 July 2011	
ENVISAT	GDR v2.1	6 to 113	14 May 2002 to 8 April 2012	
TOPEX/POSEIDON	M-GDR	1 to 481	25 September 1992 to 8 October 2005	
JASON-1	GDR	1 to 525	15 January 2002 to 15 February 2013	Mission going on
JASON-2	GDR	0 to 168	4 July 2008 to 1 February 2013	Mission going on
GEOSAT FOLLOW ON (GFO)	GDR	37 to 222	7 January 2000 to 7 September 2008	
CRYOSAT-2	IGDR	11 to 580	28 January 2011 to 8 April 2013	Mission going on

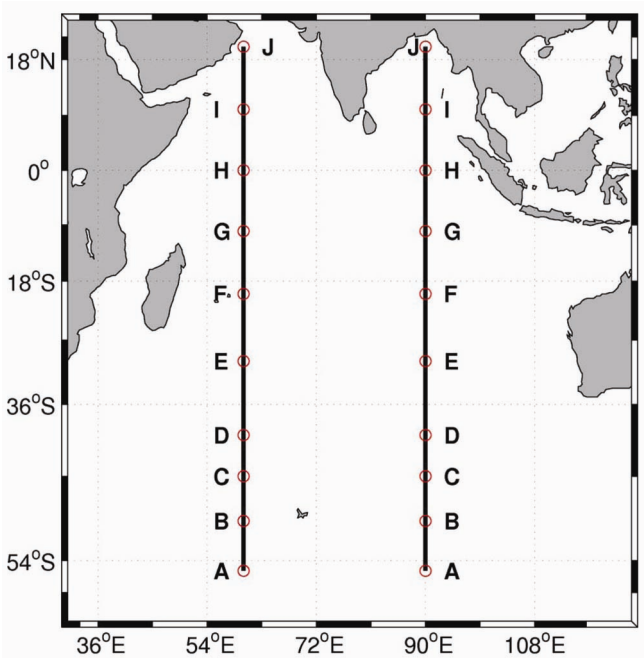

Figure 1. Study domain and plane of transects in the Arabian Sea and the Bay of Bengal.

cycle orbit. The phases A and B have 3-day repeat cycle, whereas phases E and F have a 168-day repeat cycle (Table 1). The ERS-2 mission has temporal data coverage for almost 16 years and 2 months. More details on the ERS-1 and ERS-2 missions are available in CERSAT[19]. The TOPEX-POSEIDON mission has data repository on Merged Geophysical Data Record (M-GDR) for almost 13 years. The JASON-1 mission had GDR from cycle 1 (15 January 2002) to cycle 525 (15 February 2013). One can find comprehensive validation checks for SWH derived from JASON-1/2 with *in situ* buoy records in the work by Queffeulou[20]. The JASON-2 mission has data availability for 4 years and 7 months and the mission is still ongoing. The cycle '0' in JASON-2 mission corresponds to (4 July 2008) and '168' (1 February 2013). The source of CRYOSAT data is from the NOAA Laboratory for Satellite Altimetry, USA. More details on the data quality and validation check of satellite-derived parameters from CRYOSAT are available in Queffeulou[21].

Data from the above-mentioned eight satellite missions are available for the global oceans. The region of interest in the present study is the Indian Ocean basin bounded by the geographic coordinates 30°E–120°E; 30°N–60°S as shown in Figure 1. The satellite records contain binary data format converted into text files using the Basic Radar Altimetry Toolbox (BRAT) version 3.1.0. The BRAT comprises three different filters, viz. smooth, extrapolate and loess with functionality of smoothing, filling data gaps and combination of both respectively. The processed daily data contains parameters such as MSWH (in m) and MWS (in m s^{-1}) for the above-mentioned study domain. Two transects (one along 60°E and other along 90°E) were chosen that cover the western and eastern portion of the Indian Ocean basin. For each transect ten locations (A–J) identify the regions of extra-tropical, equatorial and tropical belts in the Indian Ocean. More precisely these ten locations cover the regions of South Indian Ocean, south sub-tropical, south trade wind, equatorial and tropical northeast and northwest Indian Ocean sectors. Variability of MWS and MSWH along these ten locations was studied to understand the trends in wind-wave climate. The periods corresponding to cyclones and depressions in the past 21 years for the entire study domain are not accounted in final data analysis. Table 2 shows the year-wise count distribution on the number of cyclones filtered out in the Arabian Sea and Bay of Bengal regions along two transects as defined in Figure 1. The historical record for the best cyclone track from the Joint Typhoon Warning Centre (JTWC) provides the number of cyclones and their corresponding track details. The archived JTWC database contains the record of cyclones from 1945 to present, covering regions of SO and North Indian Ocean (NIO). As seen from Figure 1, the two transects cover only areas of deep water as data quality measured by satellites is prone to errors in shallow and near-shore areas. The subsequent section deals with the data quality, calibration, and validation

checks performed on the altimeter data used for the present study.

Validation checks for multi-platform satellite altimeter data

Quality controlled long-term data is an essential prerequisite for wind-wave climate studies. As mentioned above, on basin scales the measured data from *in situ* observing platforms are limited. Therefore, one has to depend upon model or satellite products to understand the variability for large spatial areas over the oceans. Several studies have utilized satellite products that merges multi-satellite altimeter data to process sea-level and monitor ocean circulation[22,23]. Their study opened new avenues for oceanographic studies utilizing satellite data combining altimeter data from TOPEX/Poseidon, ERS-1/2, GFO, ENVISAT and JASON-1. Recently, Shanas *et al.*[24] compared multi-mission satellite altimeter derived wave heights with buoy data for the Indian seas. This signifies that monthly averaged buoy and altimeter wave heights had a very good correlation. Queffeulou[25] reported the long term validation of altimeter wave heights from multi-satellite missions. He used data from six altimeter missions since July 1991, to check the consistency and homogeneity of the data, based on comprehensive validation checks using cross-altimeter and buoy observations. His work led to the development of a consistent and homogeneous research quality data. Many other studies also report the validation and calibration of satellite altimetry wave heights. These include the validation of JASON-1 and ENVISAT wave heights[26], assessment of global statistics for JASON-2 and cross-calibration with JASON-1 (ref. 27), validation of JASON and TOPEX satellite data with buoy and model comparisons[28], and calibration of wave measurements by TOPEX, JASON-1/2 (ref. 29). All these studies bring to light that as time progresses satellite-derived products have undergone thorough calibration and validation checks leading to the development of homogeneous research quality data. The point of focus is that data used to understand the trends in wind-wave climate utilized altimeter data that had already undergone rigorous calibration and validation checks with the other *in situ* observations. In general, the altimeter derived MSWH is a quality product beyond doubt that aids one to deduce meaningful conclusions.

Table 2. Year-wise distribution of the number of cyclone tracks and data filtered for the Arabian Sea and the Bay of Bengal region

Arabian Sea		Bay of Bengal	
Year	Number of cyclones	Year	Number of cyclones
1992	4	1992	7
1993	3	1993	3
1994	6	1994	3
1995	3	1995	3
1996	8	1996	7
1997	1	1997	5
1998	4	1998	6
1999	3	1999	4
2000	2	2000	3
2001	1	2001	2
2002	7	2002	2
2003	5	2003	3
2004	5	2004	5
2005	4	2005	3
2006	3	2006	1
2007	6	2007	4
2008	4	2008	5
2009	4	2009	5
2010	2	2010	5
2011	3	2011	2
2012	4	2012	3

Results and discussion

The Intergovernmental Panel of Climate Change report clearly mentions the signs of climate change noticed across the globe[30,31]. Based on projections, the report also mentions that in future the frequency and intensity of extreme weather events are likely to increase. No comprehensive studies exist on basin wide wind-wave climate projections reported for the Indian Ocean. To display large amount of data in a meaningful manner, the representation of variable by a Hovmoller diagram provides valuable information. This representation is commonly used in the field of meteorology and oceanographic applications to handle data that vary on space-time scales. The Hovmoller plots provide information on time evolution of a scalar quantity and in the present study, the variability of MSWH. The decadal variation of daily averaged maximum wind speed as a Hovmoller diagram for the zonal belt between 40° and 60°S along the meridian (30–120°E) is shown in Figure 2. It clearly shows that wind speed in the SO belt of Indian Ocean sector has increased in the past years. The decadal variability of maximum wind speed from 2002 until present is higher than the variability seen during the period from 1992 to 2001. The conspicuous feature noticed in Figure 2 is concerning wind speed maxima that extend all along the meridian for the past one-decade (2002 until present). This wind speed maxima (core of maximum winds) show an increased activity during the current decade along the meridian. It clearly signifies that the extreme winds have increased with time for the SO belt. It has practical implications concerning the North Indian Ocean basin. It is also worthwhile to mention here that, a recent study[32] highlights swells generated from SO sector crossing the hemisphere and reaching NIO basin (in a period of ≈4 days). These swells modify as well as modulate the local wind-waves during their propagation towards the east coast of India in the Bay of Bengal region. Hence, analysis

signifies expectation of higher swell activity observed from the recent increasing trends of maximum wind speed in the SO basin. The increased swell activity and its long distance propagation confines not only to the Indian Ocean basin, but also influences other ocean basins as well. The consequences that result from an increased wind magnitude in the current decade, particularly for the SO basin are vital in terms of wave climatology for tropical NIO basin. This means an increased wave activity in NIO has direct implications on the nearshore physical oceanographic processes such as coastal erosion, sediment transport mechanisms, etc.

Figures 3 and 4 show the zonal distribution of daily averaged meridional (30–120°E) maximum SWH and MWS respectively. Figures 3 *a* and 4 *a* represent the overall basin scale (60°S–22°N) picture of maximum SWH and maximum wind speed respectively. Figures 3 *b–d* and 4 *b–d* represent the zonal distribution for the geographic coordinates bounded by (60°S–30°S); (30°S–equator) and (equator – 22°N) for MSWH and MWS respectively. The meriodional-averaged description provides a concise picture on the basin-wide variability in both space-time scales. The maximum SWH (Figure 3 *a*) shows a steady rise in wave activity for the past two decades. The core of the maxima in MSWH, and the contour slopes in the band between 60°S and 30°S (Figure 3 *b*) signify higher wave activity spread over large spatial scales in the SO belt during recent years. These findings for the current decade concur with increased wind speed activity over the SO basin (Figure 4 *a*, *b*). The trends in wind speed distribution (between 10°S and 20°S) have also increased. In general, the wind speed magnitude for regions (>10°N) in the NIO basin has increased (Figure 4 *d*) by about 2.5 m s^{-1} in the past two decades. One can observe a paradigm shift in the distribution of wind speed (Figure 4 *d*) for the NIO basin in the last one decade (2001 to 2012). Increased wind magnitudes are evident for equatorial regions (Figure 4 *c*, *d*) covering the Inter-Tropical Convergence Zone (ITCZ) during the current decade (from 2001). The ITCZ is a region of convergence where the northeast and southeast trade winds normally converge. Both these systems of trade winds along ITCZ show an increased activity from 2001 to 2012. The highest impact of climate change is apparent in the Southern Ocean region (the band extending from 40°S to 60°S). A time series animation of the wave activity from the post-processed BRAT data (figure not shown here) clearly shows the northward migration of MSWH from the SO basin towards the tropical belt. Based on this analysis, the distribution of wind-waves (Figures 3 *c* and 4 *c*) in the tropical regions is not synchronized unlike that seen for SO basin. We believe that wind direction could be a parameter that has a direct bearing on this anomalous behaviour and requires further study.

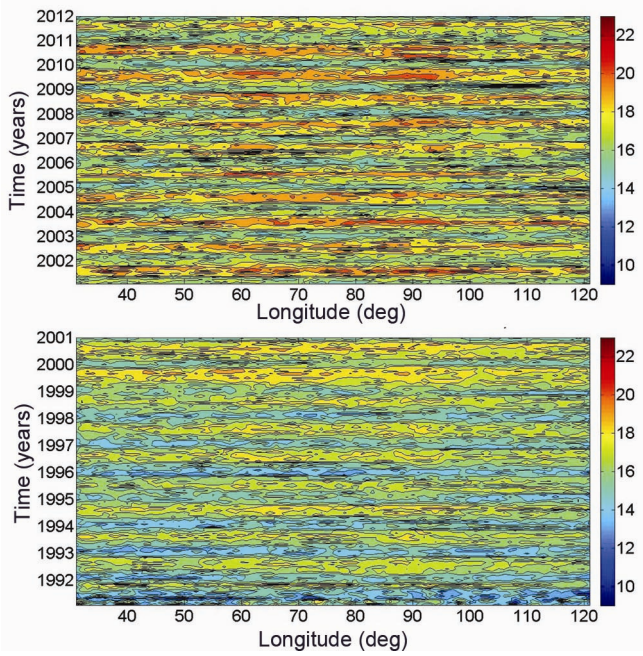

Figure 2. Decadal variation of zonally averaged maximum wind speed between the geographic coordinates 40°S–60°S in the southern belt of the Indian Ocean.

A recent study on the wave projections used five independent wave models to show that wave heights will increase in the seas off Indonesia, Antarctica and east coast of Australia[1]. In the context of the Southern Ocean, one can expect a shift in the Southern Annual Model (SAM) that strengthens the westerly wind patterns in the Southern Ocean sector. Therefore, increased wave activity in this region influences swell propagation in the northward direction that reaches other ocean basins. Their study also points out the possibility of decreased wave heights in other regions especially for the Northern Hemisphere, arising due to the effect of climate change in the coming century. In the context to the Indian Ocean sector, increased wave activity due to climate change has implications on fishing industry and coastal mitigation measures. Figures 5 and 6 depict the trend distribution of meriodional averaged MSWH and MWS respectively. Table 3 provides additional information on basin-wide variability of wind-waves for both the Arabian Sea and Bay of Bengal for the past two decades. The analysis shown in Table 3 corresponds to transect at Arabian Sea and the Bay of Bengal as shown in Figure 1, and confines to the analysis of the meriodional-averaged band for the Arabian Sea (55°E–65°E) and for the Bay of Bengal (85°E–95°E). For each zonal band, the numerical values (both wind and waves in Table 3) represent the incremental difference between 1992 until 2012. The solid linear line in each panel (Figures 5 and 6) is the best-fit regression equation pertaining to variability of the wind-waves for the Indian Ocean basin. In the SO (55°S latitude) basin there is an overall increased wave activity by almost +0.93 m in the past two decades. The trend line (Figure 5) indicates the highest maximum SWH to be

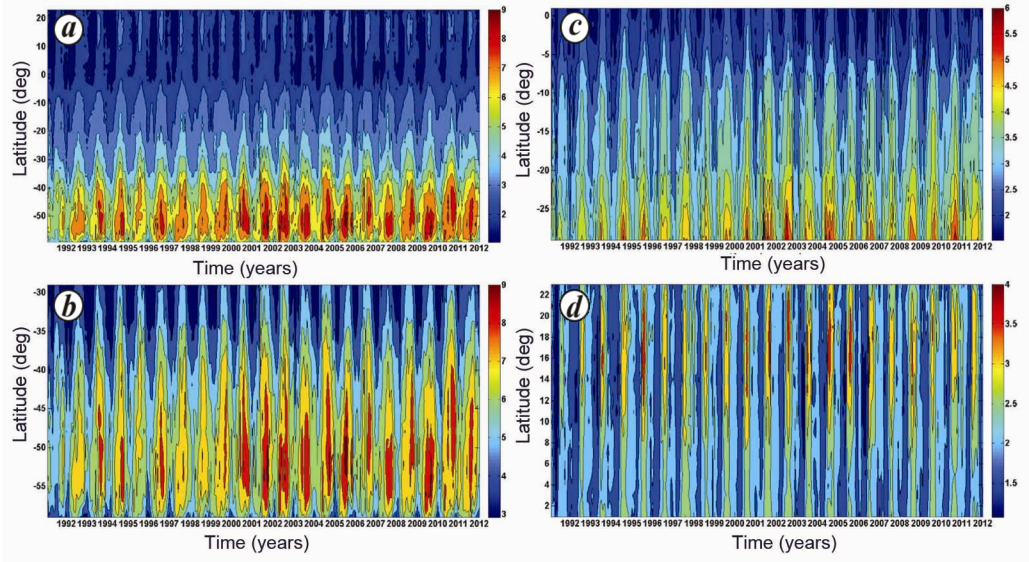

Figure 3. Hovmoller diagram of basin-scale meriodional averaged (30°E–120°E) maximum SWH (***a***) for whole Indian Ocean basin, (***b***) between 60°S and 30°S, (***c***) between 30°S and equator and (***d***) between Equator to 23°N.

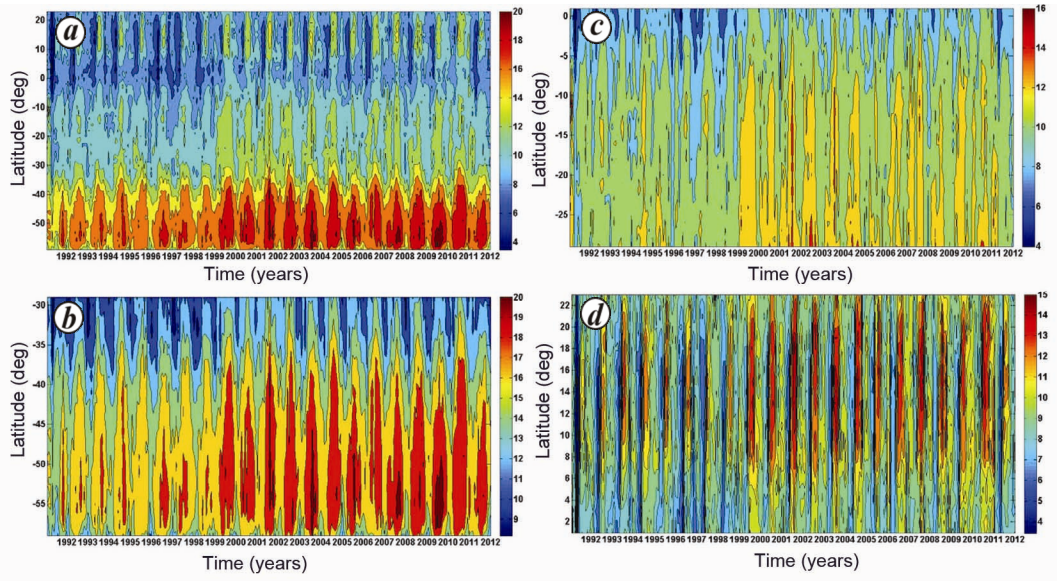

Figure 4. Hovmoller diagram of basin-scale meriodional averaged (30°E–120°E) maximum wind speed (***a***) for whole Indian Ocean basin, (***b***) between 60°S and 30°S, (***c***) between 30°S and equator and (***d***) between equator and 23°N.

about 6.6 m during 1992 increasing to 7.6 m during 2012. On an average, there is a steady rise of about +4.5 cm per year in the maximum SWH for this zone. As noticed from Table 3, the zone that experienced the highest impact during the past two decades is the extra-tropical region in SO (area covering 45°S–55°S). There is an overall increase of 1.524 m and 2.38 m s^{-1} for MSWH and MWS respectively. For eastern side of the Indian Ocean basin (transect in the Bay of Bengal corresponding to 50°S), the maximum SWH has increased by 1.427 m and wind speed by 3.16 m s^{-1} in the last two decades. Though swells circumscribe crossing the equator, the equatorial regions exhibit insignificant variation in their maximum SWH, whereas wind speed maxima showed a rise compared to the tropical South Indian Ocean. For regions in the NIO basin, wind speeds have increased by about 1.8 m s^{-1} in the last two decades. Figure 7 shows the zonal distribution of meriodional averaged MSWH and MWS respectively. In general, the zonal distribution of MSWH almost follows the trends in wind speed for both the Arabian Sea and the Bay of Bengal.

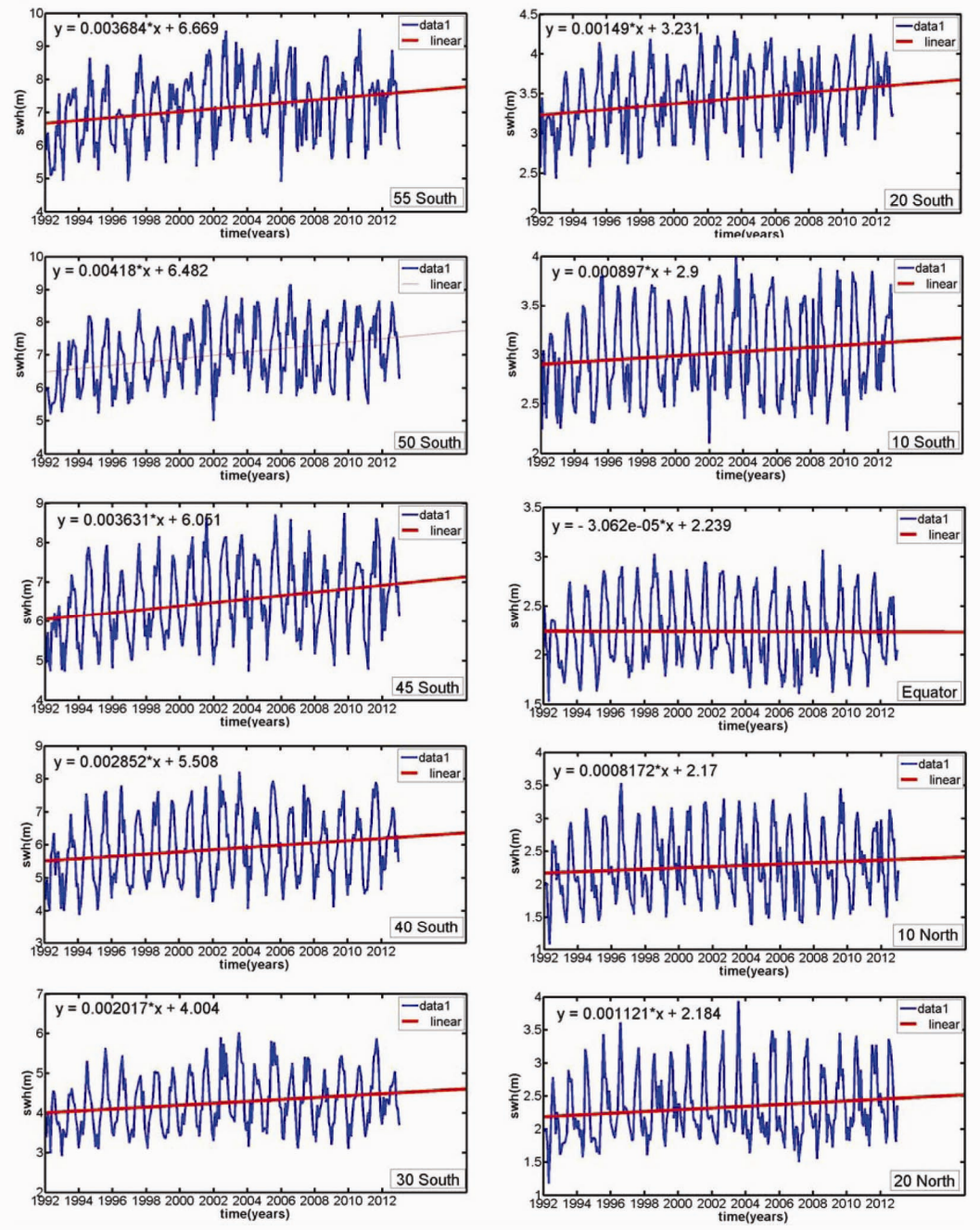

Figure 5. Zonal distribution of meriodional averaged maximum SWH (in m) between 55°S and 20°N.

For a random variable, the continuous probability distribution or the probability density function (PDF) is a measure to describe the relative likelihood of a random variable in a user defined window limit. The long term MSWH used in this analysis is a continuous random variable, and its probability within a particular range of values is the integral of its density for the given range. The PDF for a continuous random variable is a nonnegative real number. In the statistical sense, the PDF is a derivative of the cumulative distribution function or the probability mass function. To understand how the MSWH varied within a specified range of values, the PDF provides a better description on the overall distribution. The probability that a random variable like MSWH has a value between specified wave height ranges is therefore equal to the area under the probability density function bounded between the ranges. To evaluate the decadal shift in MSWH and MWS, the altimeter dataset from 1992 until 2012 were divided into two sets. The first set of data is the meriodional averaged MSWH, for the chosen ten locations (shown in Figure 1) for a period between 1992 and 2001 (10 years), and the second time series dataset

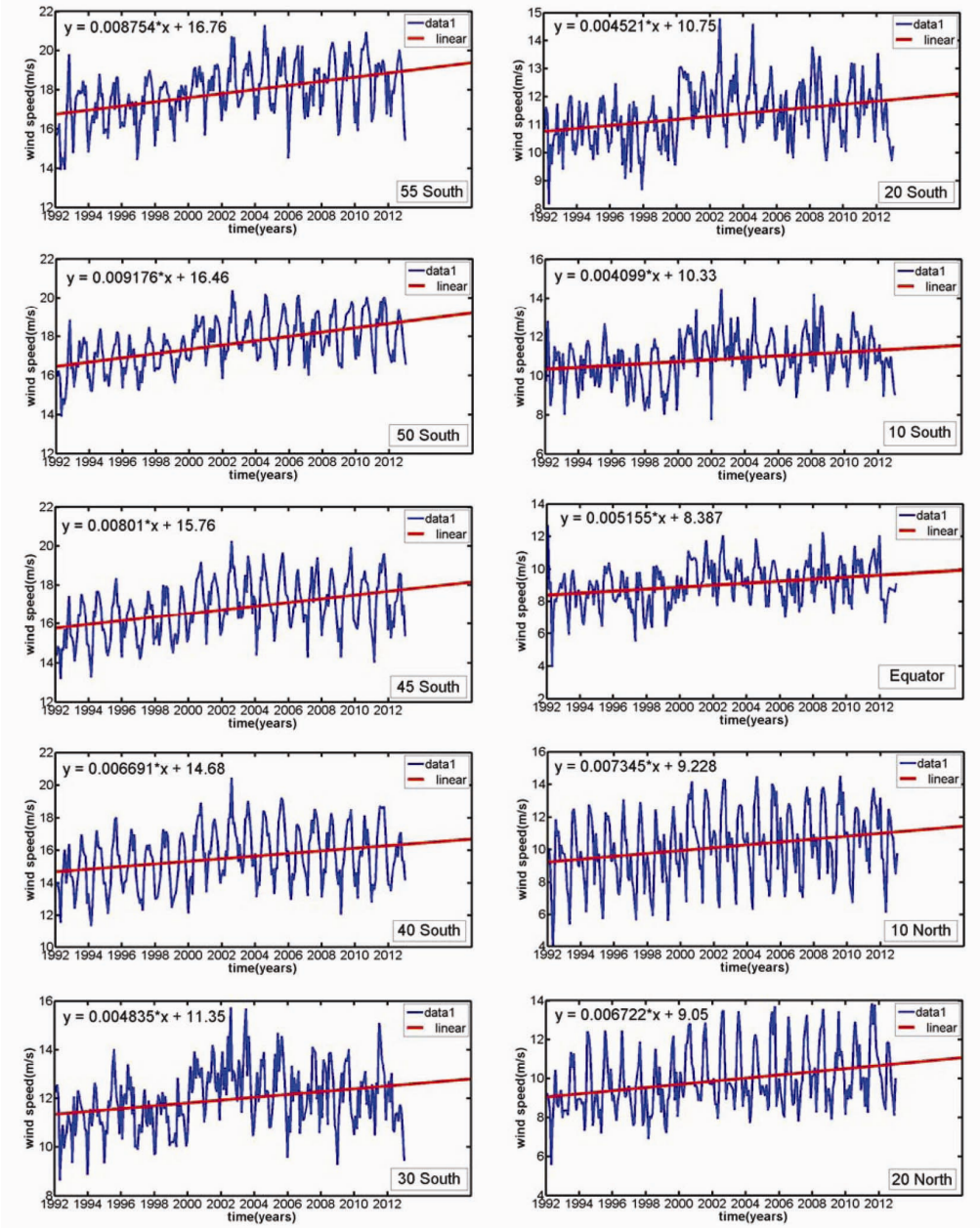

Figure 6. Zonal distribution of meriodional averaged maximum wind speed (in m s^{-1}) between 55°S and 20°N.

Table 3. Zonal variability of the maximum wind speed and maximum significant wave height between 1992 and 2012 in the Indian Ocean basin

	Arabian Sea		Bay of Bengal		Meriodional averaged	
Latitude band	Waves	Wind	Waves	Wind	Waves	Wind
55°S	0.888	2.65	0.473	1.35	0.932	2.21
50°S	0.748	2.02	1.427	3.16	1.057	2.32
45°S	1.524	2.38	0.655	1.26	0.918	2.02
40°S	0.238	2.23	0.901	1.43	0.721	1.69
30°S	0.254	0.82	0.41	0.82	0.51	1.22
20°S	0.048	0.25	0.207	0.09	0.376	1.14
10°S	0.046	1.38	0.164	0.01	0.227	1.04
Equator	0.093	1.084	0.137	1.831	–0.008	1.304
10°N	0.22	1.173	0.298	2.118	0.207	1.862
20°N	0.14	1.102	–0.02	1.07	0.283	1.7

Table 4. Test of significance based on Student's *t*-distribution with N-2 degrees of freedom (d*f*) and mean μ_x.

Latitude belt	Y-sample	Hypothesis rejection	d*f* = (*N* – 2)	Null hypothesis	α-level, *t**	*p*, *t*-test
20°N	MSWH	YES	250	Slope = 0	(5%, 1.969)	(0.0106, 2.5734)
10°N	MSWH	NO	250	Slope = 0	(5%, 1.969)	(0.0749, 1.7886)
Equator	MSWH	NO	250	Slope = 0	(5%, 1.969)	(0.9212, –0.0990)
10°S	MSWH	YES	250	Slope = 0	(5%, 1.969)	(0.0192, 2.3561)
20°S	MSWH	YES	250	Slope = 0	(5%, 1.969)	(0.00004, 4.1520)
30°S	MSWH	YES	250	Slope = 0	(5%, 1.969)	(0.00074, 3.4152)
40°S	MSWH	YES	250	Slope = 0	(5%, 1.969)	(0.0013, 3.2446)
45°S	MSWH	YES	250	Slope = 0	(5%, 1.969)	(0.00001, 4.4868)
50°S	MSWH	YES	250	Slope = 0	(5%, 1.969)	(1.02E-07, 5.481)
55°S	MSWH	YES	250	Slope = 0	(5%, 1.969)	(1.50E-05, 4.415)

MSWH, Maximum significant wave height.

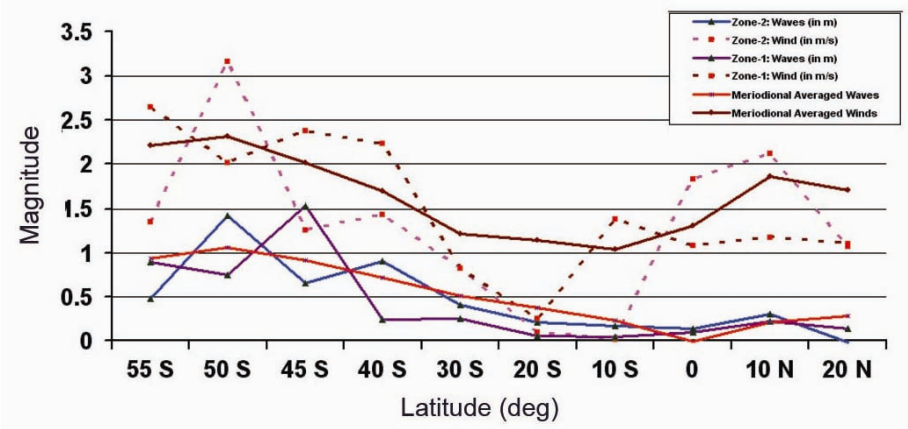

Figure 7. Zonal distribution of meriodional averaged MSWH and MWS for the respective ten locations (Zone-1 in Arabian Sea and Zone-2 in Bay of Bengal as shown in Figure 1).

corresponds to the period from 2002 to 2012. Figure 8 shows the probability distribution function using these two datasets. The *X*-axis denotes the MSWH range and the *Y*-axis the corresponding distribution of probability density. The dotted lines represent the best log-normal fit using the decadal datasets with 95% confidence level of significance. A notable observation in Figure 8 is that the probability density of higher waves has increased in the recent decade (2002–2012) compared to the 1990s. The probability density distribution reveals the lower range of MSWH during 1990s to be higher compared to the present decade. A reversing trend was noticed in the decadal variation of MSWH on comparing the lower and higher ranges of wave height. It means the statistical distribution of higher waves during 1990s was lower during the current decade and vice-versa. There is a significant and clear observational support on the rise in higher range of MSWH in the present decade unlike the period during the early 1990s. This reversing trend occurs along the ten stations in the Indian Ocean sector. A marginal difference was noticed for regions along the equatorial belt and for regions in the North Indian Ocean, a rise in the higher range of MSWH was observed. Table 4 lists the test of significance based on Student's *t*-distribution to assess the statistical significance of all the trends for MSWH observed in Figure 5. The null hypothesis of zero-slope is rejected for cases at 5% level of significance with 95% confidence interval. As noticed from Table 4, the regions of highest variability in MSWH are from the Southern Ocean sector of the Indian Ocean with a marginal variability noticed for the equatorial regions.

Summary and conclusions

The objective of this present study was to understand the recent trends in MSWH and associated MWS for the Indian Ocean basin based on observational evidence. The inferences are based on a comprehensive analysis of all available altimeter data from eight altimeter missions, viz. ERS-1/2, TOPEX-POSEIDON, GEOSAT Follow-ON (GFO), JASON-1/2, ENVISAT and CRYOSAT products. Preliminary analysis of altimeter data using BRAT revealed that MSWH activity shows a pronounced increase in the SO basin. High waves generated in the extra-tropical belt of SO migrate northwards reaching the NIO crossing the hemisphere. Likewise, an increasing trend was observed for the wind magnitude especially in the

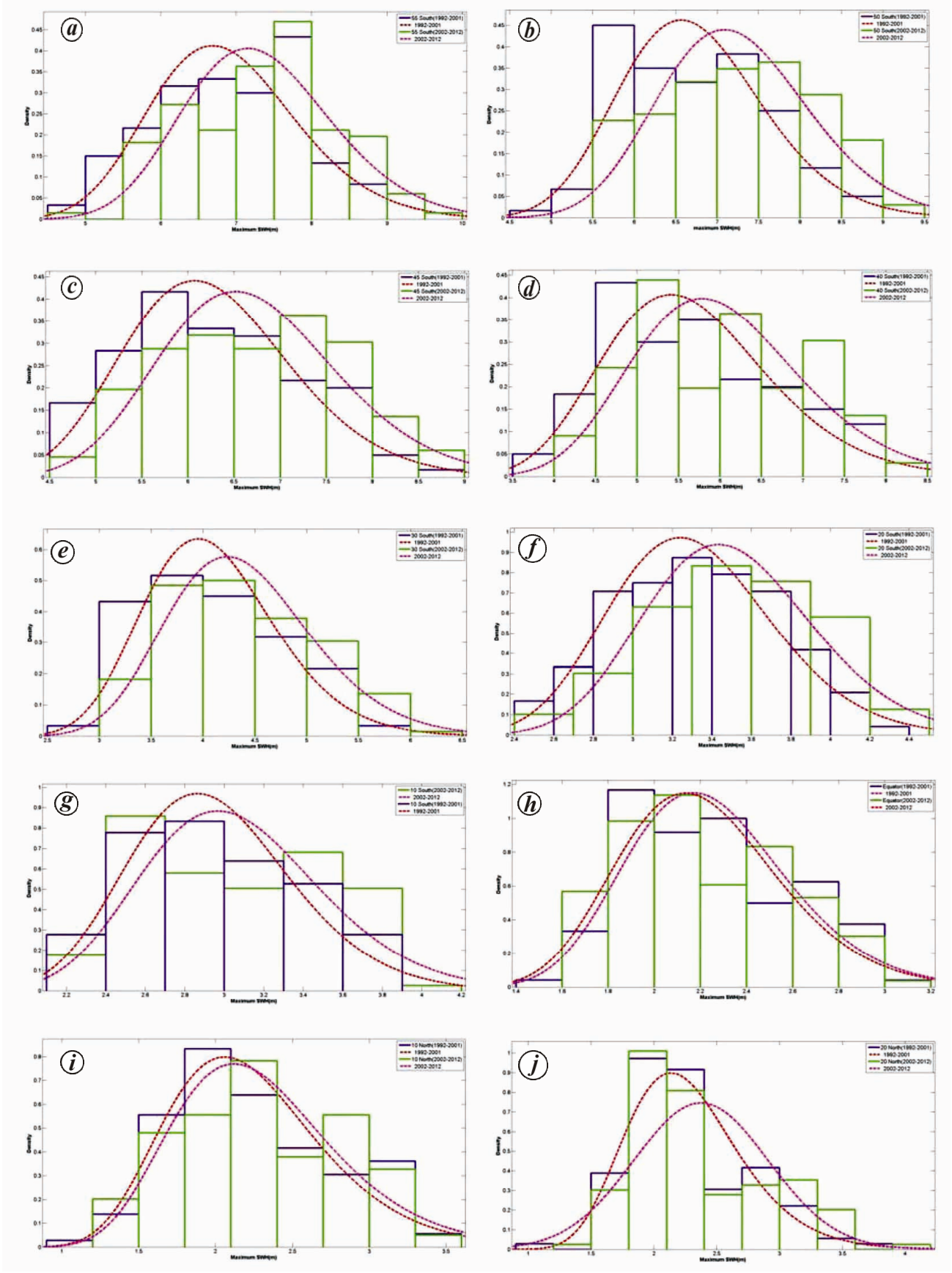

Figure 8. Probability density function along various latitudinal sections.

SO basin, and this rise was substantial in the current decade. Analysis for the two transects, one for the Arabian Sea and the other for the Bay of Bengal basin also showed that regions in the NIO basin experienced an increasing trend during the past two decades. In a quantitative sense, the SO belt (between 45°S and 55°S) experienced the highest variability of MSWH in the last two decades. This zone showed a steady rise of about 7.2 cm year^{-1} and 0.12 m s^{-1} year^{-1} for MSWH and MWS respectively. The observed variability was quite marginal for the equatorial regions, whereas the MWSH and MWS for the NIO basin showed an increasing trend of +1.5 cm year^{-1} and 0.09 m s^{-1} year^{-1} respectively. In an engineering perspective, increased trends observed in MSWH needs to be accounted during the design stage and procedural planning for coastal and offshore structures.

1. Gulev, S. K., Grigorieva, V., Sterl, A. and Woolf, D., Assessment of the reliability of wave observations from voluntary observing ships: Insights from the validation of a global wind wave climatology based on voluntary observing ship data. *J. Geophys. Res. Oceans*, 2003, **108**(C7), 3236; doi: 10.1029 /2002JC001437.
2. Hemer, M. A., Church, J. A. and Hunter, J. R., Variability and trends in the directional wave climate of the Southern Hemisphere. *Int. J. Climatol.*, 2010, **30**, 475–491.
3. Young, I. R., Zieger, S. and Babanin, A. V., Global trends in wind speed and wave height. *Science*, 2011, **332**, 451–455.
4. Gower, J. F. R., GEOS-3 Ocean wave measurements in Northeast Pacific. *Trans. Am. Geophys. Union*, 1976, **57**(12), 944.
5. Chelton, D. B., Hussey, K. J. and Parke, M. E., Global satellite measurements of water vapor, wind speed and wave height. *Nature*, 1981, **294**, 529–532.
6. Challenor, P. G., Foale, S. and Webb, D. J., Seasonal changes in the global wave climate measured by the GEOSAT altimeter. *Int. J. Remote Sensing*, 1990, **11**, 2205–2213.
7. Carter, D. J. T., Foale, S. and Webb, D. J., Variations in global wave climate throughout the year. *Int. J. Remote Sensing*, 1991, **12**, 1687–1697.
8. Yang, J. *et al.*, The role of satellite remote sensing in climate change studies. *Nature Clim. Change*, 2013; doi: 10.1038/ nclimate1908.
9. Hemer, M. A., Fan, Y., Mori, N., Semedo, A. and Wang, X. L., Projected changes in wave climate from a multi-model ensemble. *Nature Clim. Change*, 2013, **3**, 471–476.
10. Wang, X. L., Zwiers, F. W. and Swail, V. R., North Atlantic Ocean wave climate change scenarios for the twenty-first century. *J. Climate*, 2004, **17**, 2368–2383.
11. Wang, X. L. and Swail, V. R., Climate change signal and uncertainty in projections of ocean wave heights. *Climate Dynamics*, 2006, **26**, 109–126.
12. Shimura, T., Mori, N., Tom, T., Yasuda, T. and Mase, H., Wave climate change projection at the end of 21st century. Proceedings of the International Conference on Coastal Engineering, Shanghai, China, 2010.
13. Mori, N., Yasuda, T., Mase, H., Tom, T. and Oku, Y., Projection of extreme wave climate change over global warming. *Hydrol. Res. Lett.*, 2010, **4**, 15–19.
14. Renske, C. W., Sterl, A., deVries, J. W., Weber, S. L. and Ruessink, G., The effect of climate change on extreme waves in front of the Dutch coast. *Ocean Dynamics*, 2012; doi 10.1007/s10236-012-0551-7.
15. Snodgrass, F. E., Groves, G. W., Hasselmann, K., Miller, G. R., Munk, W. H. and Powers, W. H., Propagation of ocean swell across the Pacific. *Philos. Trans. R. Soc. London*, 1966, **249A**, 431–497.
16. Sterl, A. and Caires, S., Climatology, variability and extrema of ocean waves: the web-based JNMI/ERA-40 wave atlas. *Int. J. Climatol.*, 2005, **25**(7), 963–977.
17. Naeije, M. C., Schrama, E. J. O. and Scharroo, R., The radar Altimeter Database System project RADS. In Proceedings of the IGARSS 2000 Conference (eds Tammy, I. S.), Hawaii, 24 July 2000, 2000, pp. 487–490.
18. Queffeulou, P., Ardhuin, F. and Lefevre, J. M., Wave height measurements from altimeters: validation status and applications, OSTST Meeting, San Diego, 19–21 October 2011.
19. CERSAT, *Altimeter and Microwave Radiometer ERS Products User Manual*, C2-MUTA-01-1F, Version 2.2, IFREMER, BP 70, 29280, France, 1996.
20. Queffeulou, P., Preliminary assessment of Jason-2 GDR version D for SWH and Sigma-0 data, Report, 2012, September 2012, p. 3.
21. Queffeulou, P., Cryosat-2 IGDR SWH assessment update, Report, 2013, May 2013.
22. Le Traon, P. Y., Nadal, F. and Ducet, N., An improved mapping method of multisatellite altimeter data. *J. Atmos. Oceanic Technol.*, 1998, **15**, 522–533.
23. Le Traon, P. Y., Dibarboure, G. and Ducet, N., Use of a high-resolution model to analyze the mapping capabilities of multiple altimeter missions. *J. Atmos. Oceanic Technol.*, 2002, **18**, 1277–1288.
24. Shanas, P. R., Sanil Kumar, V. and Hithin, N. K., Comparison of gridded multi-mission and along-track mono-mission satellite altimetry wave heights with *in situ* near-shore buoy data. *Ocean Eng.*, 2014, **83**, 24–35.
25. Queffeulou, P., Long-term validation of wave height measurements from altimeters. *Mar. Geodesy*, 2004, **27**, 495–510.
26. Durrant, T. H., Greenslade, D. J. M. and Simmonds, I., Validation of Jason-1 and Envisat remotely sensed wave heights. *J. Atmos. Oceanic Technol.*, 2009, **26**, 123–134.
27. Ablain, M., Philipps, S., Picot, N. and Bronner, E., Jason-2 global statistical assessment and cross-calibration with Jason-1. *Mar. Geodesy*, 2010, **33**, 162–185.
28. Ray, R. D. and Beckley, B. D., Simultaneous ocean wave measurements by the Jason and Topex satellites, with buoy and model comparisons. *Mar. Geodesy*, 2003, **26**, 367–382.
29. Ray, R. D. and Beckley, B. D., Calibration of ocean wave measurements by the TOPEX, Jason-1, and Jason-2 satellites. *Mar. Geodesy*, 2012, **35**, 238–257.
30. IPCC, Climate Change 2007: The Physical Science Basis. Contribution of Working Group I to IV Assessment Report of the Intergovernmental Panel on Climate Change (eds Solomon S. *et al.*). Cambridge University Press, 2007, Cambridge, UK, p. 996.
31. IPCC, Changes in climate extremes and their impacts on the natural physical environment: An overview of the IPCC SREX report. Seneviratne, S. I. *et al.*, EGU Gen. Assembly 2012, 22–27 April 2012, Vienna, Austria, p. 12566.
32. Nayak, S., Bhaskaran, P. K., Venkatesan, R. and Dasgupta, S., Modulation of local windwaves at Kalpakkam from remote forcing effects of Southern Ocean swells. *Ocean Eng.*, 2013, **64**, 23–35.

Received 24 September 2014; revised accepted 23 March 2015